Machinability of Free-cutting Leaded Steels

By

Keiji OKUSHIMA* and Kazuaki IWATA*

(Received October 20, 1961)

The machinability of free-cutting leaded steel was investigated from the viewpoint of tool life, surface finish, cutting force and chip formation.

Orthogonal and conventional cutting tests were performed for nine grades of leaded steel and four grades of non-leaded steel in order to determine the effect of including lead in steel. The addition of lead to steel was found effective in improving the machinability.

The cutting mechanism of free-cutting leaded steels was analysed based upon the flow region concept. The effects of depth of cut and lead content on the cutting process were discussed. It was found that a smoother shear deformation occurs in the cutting process for leaded steels than for non-leaded steels, and hence the inclusion of lead in steels improves machinability.

1. Introduction

Machinability is one of the important factors in the machine shop. The term machinability has been defined by many investigators. In this paper, the authors define the term as the ease of machining metals with various tool grades; that is,

1. Tool life
2. Surface finish
3. Cutting force and power consumption
4. Chip formation and type of chip

Tool life is determined by the wear on the face or flank of a cutting tool, expressed as the cutting time before the tool is resharpened. Surface finish is related to the clearance of two machine parts and is expressed in terms of the roughness, accuracy and quality of the machined surface. Cutting force and power consumption in metal cutting are related to the machining ability of the lathe. Formation of chips and the type of chip are important in metal cutting from the standpoint of machinability.

This paper deals with experimental results on the machinability of free-cutting leaded steels in terms of the above four meanings of machinability.

* Department of Precision Mechanics

Table 1. Chemical compositions of test materials

Materials	Chemical composition									
Grades	C	Si	Mn	P	S	Cu	Ni	Cr	Mo	Pb
S45CF-A	0.46	0.24	0.69	0.016	0.014	0.19	0.11	0.14	—	—
S45CF-B	0.47	0.25	0.74	0.021	0.016	0.26	0.11	0.07	—	—
S45CF-E	0.47	0.24	0.70	0.019	0.009	0.22	0.17	0.12	—	0.18
S45CF-F	0.46	0.23	0.69	0.015	0.008	0.23	0.13	0.07	—	0.19
S45CF-G	0.47	0.25	0.69	0.016	0.010	0.24	0.11	0.10	—	0.19
S45CF-H	0.46	0.21	0.72	0.029	0.008	0.25	0.16	0.12	—	0.14
S45CF-K	0.48	0.26	0.68	0.021	0.015	0.21	0.11	0.09	—	0.14
SCM22-C	0.19	0.33	0.74	0.022	0.013	0.20	0.10	0.99	0.19	—
SCM22-D	0.19	0.21	0.69	0.020	0.009	0.22	0.10	1.13	0.19	—
SCM22F-M	0.21	0.17	0.70	0.021	0.009	0.20	0.08	1.14	0.18	0.19
SCM22F-X	0.20	0.21	0.73	0.017	0.008	0.22	0.07	1.01	0.18	0.10
SCM22F-Y	0.21	0.22	0.77	0.024	0.008	0.22	0.12	0.95	0.19	0.15
SCM22F-Z	0.18	0.20	0.69	0.013	0.009	0.19	0.05	1.03	0.18	0.20

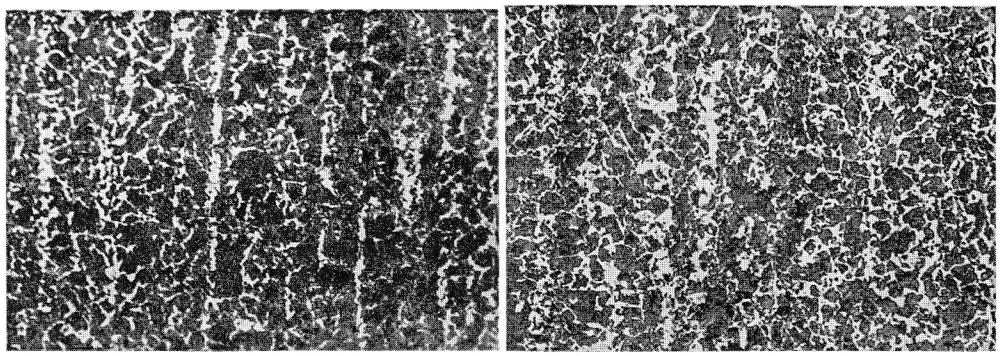

(a) S45C-B　　(b) S45CF-E

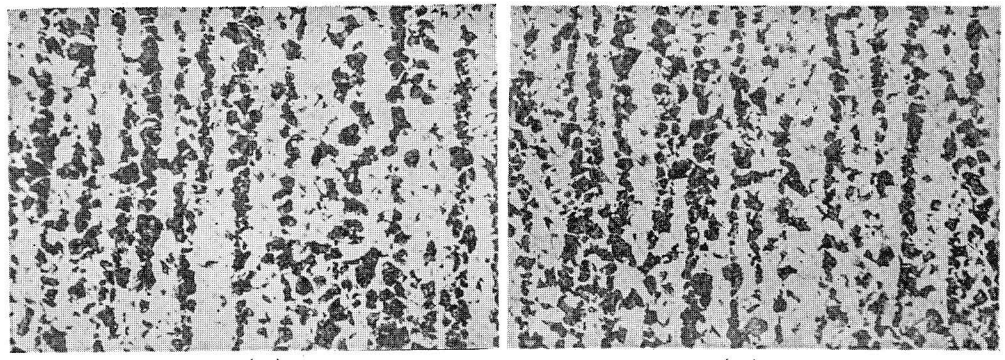

(c) SCM22-C　　(d) SCM22F-M

Fig. 1. Microstructures of test materials (×100)

2. Microstructures and properties of free-cutting leaded steels tested

13 grades of free-cutting leaded steel; that is, seven grades of S45C steel and six grades of SCM22 steel, were tested. The chemical compositions of these materials are shown in Table 1. Fig. 1 shows the microstructures of these materials and Fig. 2 shows typical examples of electron microscope photomicrographs of the test materials. It is evident from these photomicrographs that grades of S45C consist of ferrite and pearlite, while grades of SCM22 steel show band structures of ferrite and pearlite. Table 2 shows the sizes of these structures. Fig. 3 shows a typical photograph of the lead which is included in S45CF

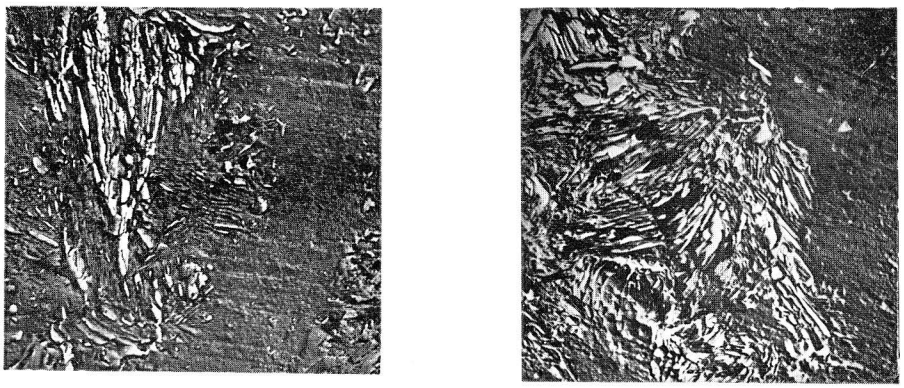

SCM22-D SCM22F-Y

Fig. 2. Typical examples of photomicrographs of electron microscope (×2400)

Table 2. Size of test materials

Materials	rough grain (%)		fine grain (%)		number
S45C-A	4.0	14%	6.3	86%	5.9
S45C-B	4.0	6%	6.4	94%	6.3
S45CF-E	4.0	4%	6.4	96%	6.3
S45CF-F	4.0	10%	6.3	90%	6.1
S45CF-G	4.0	8%	6.4	92%	6.2
S45CF-H	4.0	8%	6.3	92%	6.1
S45CF-K	4.0	18%	6.1	82%	5.6
SCM22-C	—		100%		7.2
SCM22-D	2.3	66%	5.8	34%	3.5
SCM22F-M	1.8	54%	6.5	46%	4.6

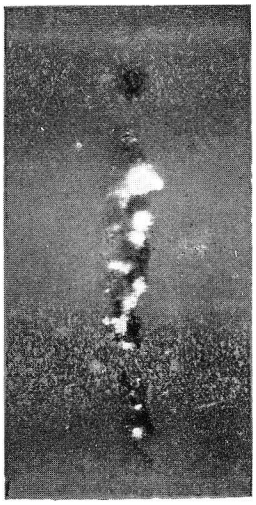

Fig. 3. Typical photograph of lead. (Included in S45CF steels) (×800)

steels. In this photograph, the white spots appear to be lead and the dark areas are non-metallic inclusions.

Mechanical properties, such as Brinell hardness number, yielding point, tensile strength, elongation, contraction, and the impact values of leaded steels and non-leaded steels are compared in Table 3.

Table 3. Mechanical properties of test materials

Materials	Mechanical properties						
	Yielding point	tensile strength	Elongation	Contraction	Hardness	Impact value	Hardness after normalizing
S45C-A	60	78	25	61	223	18	198
S45C-B	65	78	27	60	241	17	202
S45CF-E	62	79	26	57	223	13	207
S45CF-F	70	82	24	56	235	14	201
S45CF-G	60	77	24	59	223	16	207
S45CF-H	65	81	26	59	223	14	202
S45CF-K	66	83	24	55	241	10	197
SCM22-C	90	99	19	46	285	14	169
SCM22-D	88	96	16	42	293	13	166
SCM22F-M	93	99	18	49	285	10	169
SCM22F-X	—	—	—	—	—	—	177
SCM22F-Y	—	—	—	—	—	—	177
SCM22F-Z	—	—	—	—	—	—	177

3. Machinability based on tool life tests

Machinability of free-cutting leaded steels was compared with that of non-leaded steels, and in these tool life tests, the lead content, cutting conditions and tool geometry were varied over a wide range.

3.1. Experimental procedure

Cutting tests were carried out dry in a high speed lathe (Niigata Iron Works Co; swing 500 mm, power 15 HP).

Tools used were steel cutting grades of carbide S-1, ST-1 and ST-2, and titanium carbides A and B.

Tool geometry is shown in Table 4. The cutting tests were stopped when

Table 4. Tool geometry in this experiment

Back-rake angle, deg	0
Side-rake angle, deg	5
End-relief angle, deg	5
Side-relief angle, deg	5
End-cutting-edge angle, deg	15
Side-cutting-edge angle, deg	15
Nose radius, mm	0.3

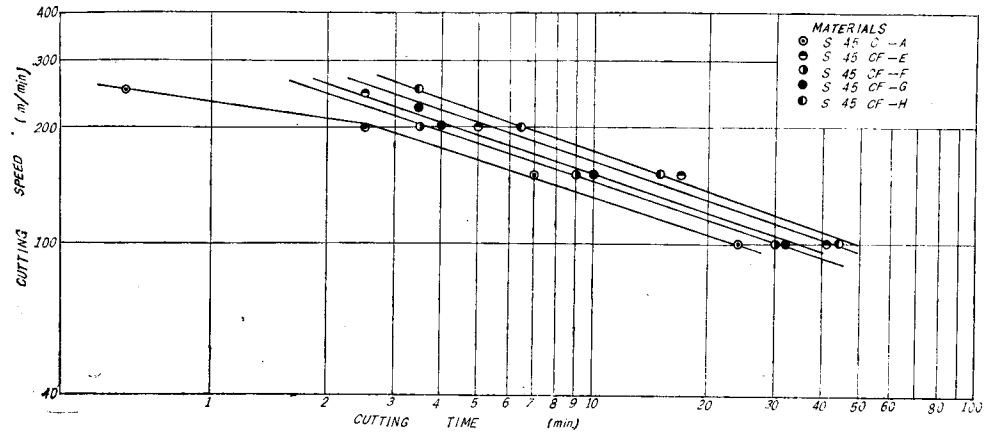

Fig. 4 (a). Tool-life plots for S45C steels of different lead contents
Cutting conditions; tool material, carbide ST-1; tool geometry, 0, 5, 5, 5, 15, 15, 0.3 mm; feed, 0.28 mm/rev; depth of cut, 1 mm; fluid, none:

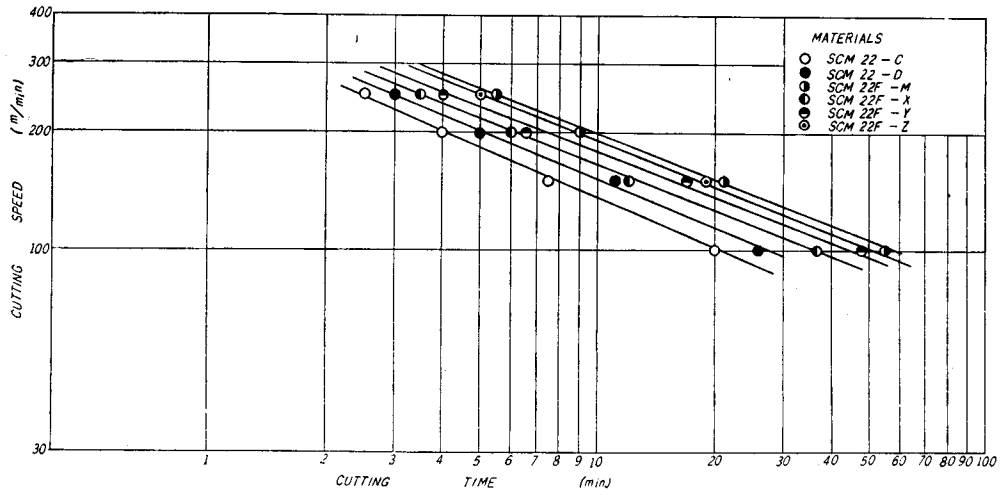

Fig. 4 (b). Tool-life plots for SCM22 steels of different lead contents
Cutting conditions; tool material, carbide ST-1; tool geometry, 0, 5, 5, 5, 15, 15, 0.3 mm; feed, 0.28 mm/rev; depth of cut, 1 mm; fluid, none;

the diameter of the test specimens became less than 40 mm due to considerations of the rigidity of the test lathe.

3. 2. Experimental results

In this experiment, the feed and depth of cut were kept constant, i.e. at 0.28 mm/rev and 1 mm respectively, and the cutting speed was varied. The tool material was carbide ST-1 grade.

The criterion of tool life in this experiment was a flank wear of 0.3 mm or a crater wear of 0.05 mm. It was found from cutting tests repeated three times under the same cutting conditions that the error of tool life data was within 20 per cent.

3. 2. 1. Tool life test

Tool life curves for five grades of leaded steel and one grade of non-leaded steel (S45C) are shown in Fig. 4(a) in relation to cutting speed. Similar tool life curves for four grades of leaded steel and two grades of non-leaded steel (SCM22) are shown in Fig. 4(b).

It is concluded from these figures that tool life depends upon the difference in tool life work materials, and that there is an especially large difference in tool life between leaded steels and non-leaded steels.

Including lead in steels greatly improved tool life without affecting the mechanical properties of steels. The effect of lead content on tool life is shown in Fig. 5. It appears that lead content affects tool life, that is, the maximum tool life was obtained for S45C with a lead content of 0.1 to 0.2%, and for SCM22 with a lead content of about 0.2%. The Taylor tool-life equation which shows the relationship between cutting speed V in m/min. and tool life T in min. corresponding to wear land of 0.3 mm is given by the following equation

$$VT^n = C \qquad \cdots\cdots\cdots\cdots (1)$$

where C and n are constants. The Taylor tool-life equations for the materials tested above are given in Table 5.

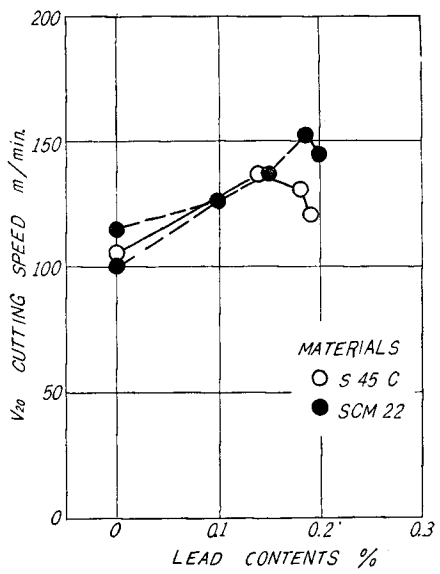

Fig. 5. Variation of V_{20} cutting speed with lead contents.

Table 5. The Taylor tool-life equations for the material tested

Materials	Taylor toor-life equation	V_{20}
S45CF-K	$VT^{0.298}=380$	135 (m/min)
S45CF-E	$VT^{0.300}=350$	129
S45CF-G	$VT^{0.308}=330$	120
S45CF-F	$VT^{0.312}=305$	115
S45C-A	$VT^{0.320}=275$	105
SCM22F-M	$VT^{0.382}=480$	152
SCM22F-Z	$VT^{0.394}=470$	145
SCM22F-Y	$VT^{0.377}=430$	137
SCM22F-X	$VT^{0.380}=410$	127
SCM22-D	$VT^{0.419}=390$	105
SCM22-C	$VT^{0.430}=360$	100

3.2.2. The selection of tool material for free-cutting leaded steels

Fig. 6 shows the tool life diagram for five grades of carbide tool tested in relation to cutting speed when cutting leaded steels.

Referring to this figure, titanium carbide shows a better tool life than steel cutting grade carbides. The order of tool life for these tool materials are: titanium carbide grade A, titanium carbide grade B, carbide grade ST-1, carbide grade S-1, carbide grade ST-2.

Experimental formulas and a cutting speed corresponding to a tool life of 20 min. (V_{20}) are listed in Table 6.

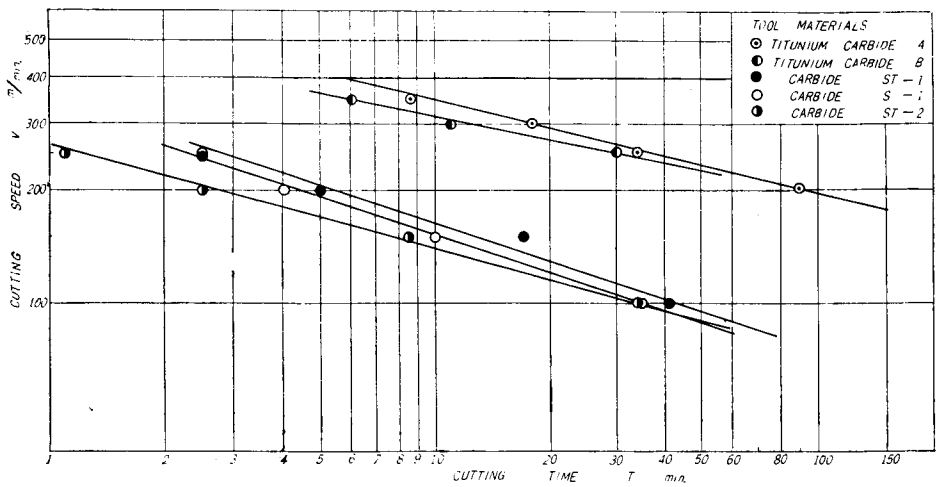

Fig. 6. Tool life plots of free-cutting leaded steel for different tool materials Cutting conditions: material, S45CF-E. Other conditions were the same as in Fig. 4.

Table 6. The Taylor tool-life equations for the tool materials

Tool materials	tool-life equation (flank)	tool-life equation (crater)	V_{20} (flank)
Titanium carbide A	$VT^{0.209}=610$	—	290
" B	$VT^{0.253}=500$	—	270
Carbide ST-1	$VT^{0.300}=350$	$VT^{0.176}=340$	129
" S-1	$VT^{0.334}=330$	$VT^{0.173}=330$	120
" ST-2	$VT^{0.273}=255$	$VT^{0.205}=275$	115

The value of n with the tool life criterion based on flank wear are larger than that based on crater wear. V_{20} for titanium carbide is twice greater than that for steel cutting grade carbide.

4. Machinability based on surface finish

Generally, the quality, acuracy and appearance of the machined surface are influenced by cutting conditions such as a cutting speed, and tool geometry.

In the following, the effects of cutting condition and lead content in the work materials on surface finish and occurence of a built-up-edge are investigated and discussed.

4. 1. Experimental procedure

Surface finish was investigated by machining nine grades of free-cutting leaded steal and four grades of non-leaded steel with a carbide tool Igetaloy ST-1 in a High-speed lathe (Ôkuma Iron Works; swing 320 mm, maximum power 3 HP). Tool geometry was (0, 5, 5, 5, 15, 15, 0.3 mm). Surface roughness was tested on a needle type optical roughness tester.

4. 2. Experimental results

Figs. 7 and 8 shows the experimental data for surface roughness when cutting speed and feed were changed 50 to 300 m/min. and 0.03, 0.06, 0.18 mm/rev, respectively.

It is well known that surface roughness increases when a built-up-edge occurs at low speeds. Even, when cutting leaded steels, the built-up-edge appeared and increased surface roughness at low speeds below 100 m/min..

The speed at which the built-up-edge disappears was determined and the results are listed in Table 7. The surface roughness approaches a constant value as the cutting speed increases. The minimum cutting speed at which surface roughness remains constant is also shown in Table 7. The critical cutting speed for built-up-edge disappearance and the cutting speed for constant surface roughness are larger for leaded steels than those for non-leaded steels. It appears that lead-included steels show an increase in the adhesion between tool and

work-materials, making it easy to generate the built-up-edge.

The critical cutting speed for built-up-edge disappearance is always a little larger than the min. cutting speed for constant surface roughness, though both followed the same trend in variation according to work materials.

Fig. 9 shows the relationship between surface finish and feed for the typical work materials tested. The relationship between coefficient of surface roughness and feed is shown in Fig. 10. Coefficient of surface roughness η is defined as follows,

$$\eta = \frac{h_{\text{act.}}}{h_{\text{theo.}}} \qquad \cdots\cdots\cdots\cdots(2)$$

where, $h_{\text{act.}}$ is the actual surface roughness

$h_{\text{theo.}}$ is the theoretical surface roughness

The effect on surface roughness of including lead in steels was not observed at low feeds but became significant at feeds above 0.18 mm/rev.

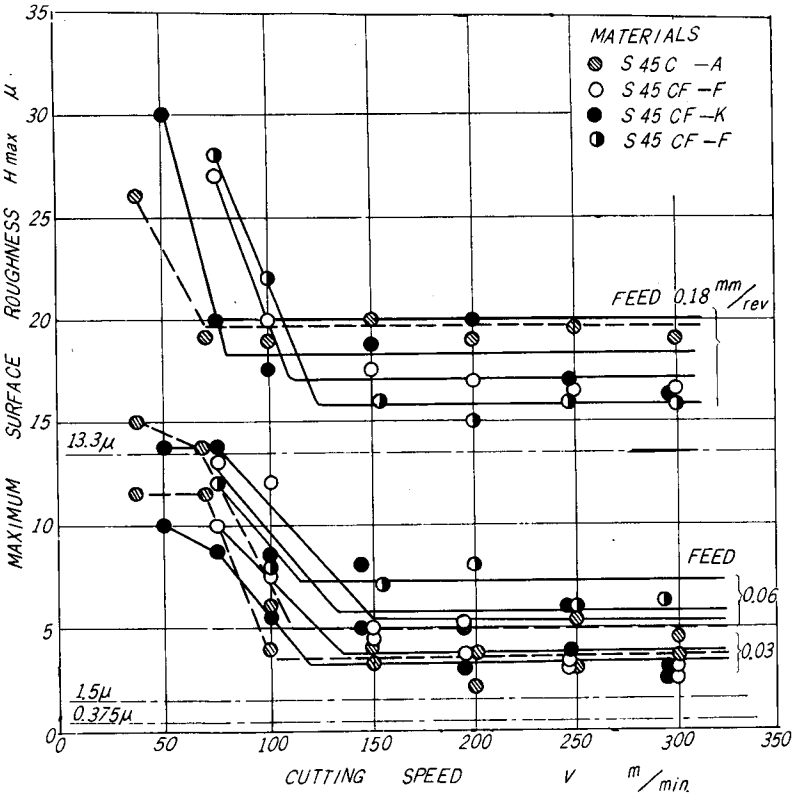

Fig. 7. Variation of maximum surface roughness with materials and cutting speed.
Cutting conditions; tool material, carbide ST-1: tool geometry, 0, 5, 5, 5, 15, 15, 0.3: depth of cut 0.5 mm; fluid, none:

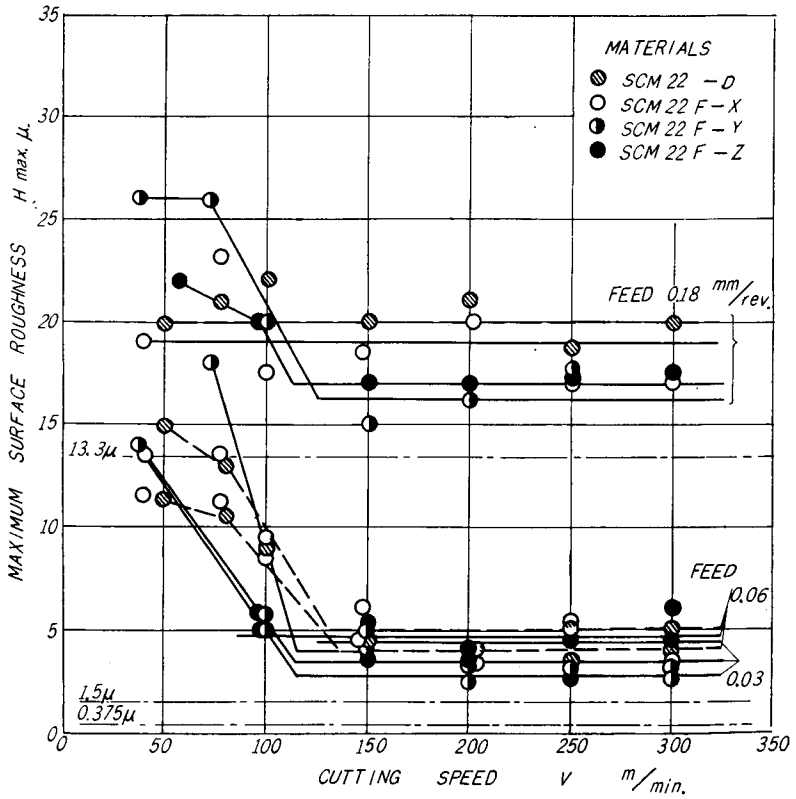

Fig. 8. Variation of maximum surface roughness with materials and cutting speed.
All other conditions were the same as in Fig. 7.

Table 7.

Materials	Critical speed for the disappearance of BUE	Critical speed for constant surface roughness S45C
S45C-A	67 (m/min)	70 (m/min)
S45CF-E	90	125
S45CF-F	80	100
S45CF-K	70	80
SCM22-D	80	90
SCM22F-X	100	100
SCM22F-Y	107	120
SCM22F-Z	95	100

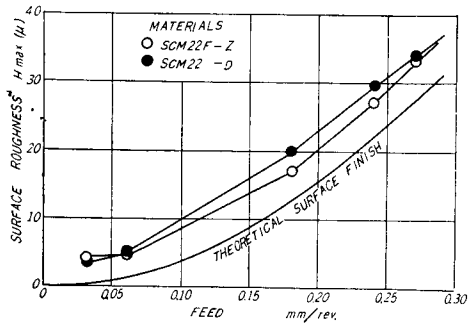

Fig. 9. Effect of feed on surface roughness.

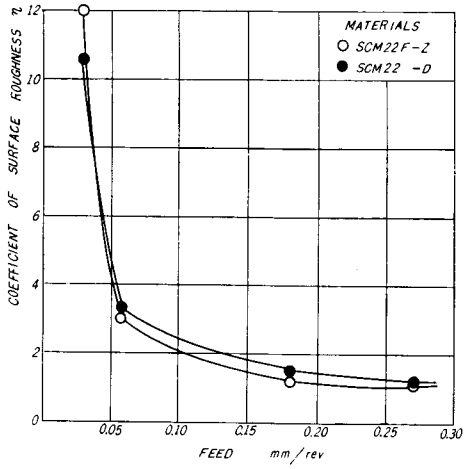

Fig. 10. Effect of feed on coefficient of surface roughness.

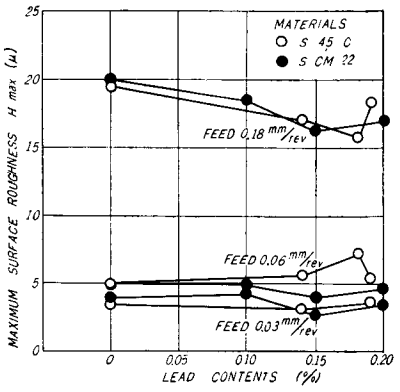

Fig. 11. Variation of H_{mxa} with lead contents.

This is shown in Fig. 11. It appears that surface roughness decreases with a lead content of 0.1 to 0.2%.

5. Machinability based on cutting force

To investigate the effect of lead addition upon cutting force, conventional (three-dimensional) cutting and orthogonal cutting were carried out.

5.1. Experimental procedure

The following equipment and cutting conditions were used.

Machine tool .....(1) High speed lathe (Niigata Iron Works)
for conventional cutting
(2) Shaper (Ôkuma Iron Works)
for orthogonal cutting

Dynamometer .....Strain gage type three-component tool dynamometer for force measurement

Tool material .....Carbide Igetaloy grade ST-1

Cutting conditions.....{ Cutting speed ; 5~250 m/min.
Feed ; 0.18, 0.28, 0.38, 0.48 mm/rev
Depth of cut ; 0.5, 1.0, 1.5 mm

5.2. Conventional cutting tests

The cutting force has a tendency to decrease with an increase in cutting speed, as shown in Figs. 12(a)(b).

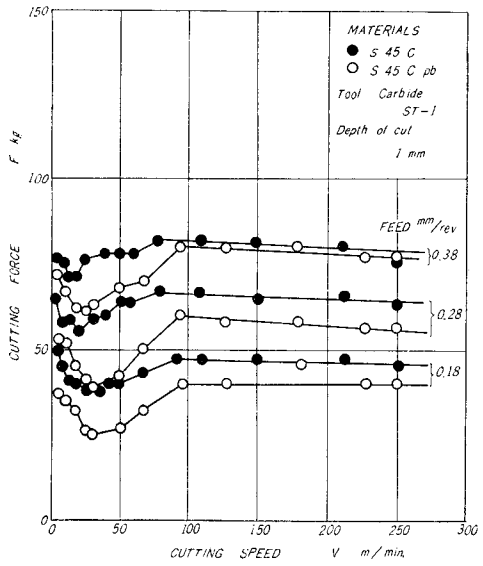

Fig. 12(a). Variation of cutting force with cutting speed and feed.

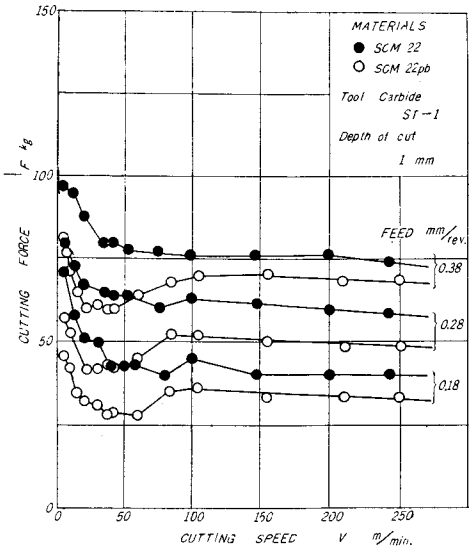

Fig. 12(b). Variation of cutting force with cutting speed and feed.

With an increase in cutting speed, the cutting force decreased in the first stage, then increased gradually from a minimum point, and reached a constant value at high speeds above some critical cutting speed. This trend was almost the same for all work materials testend except non-leaded steel SCM22 which had no evident minimum point for cutting force.

The decrease and increase in principal cutting force at low speeds below the critical cutting speed are considered to be caused by the formation of a built-up-edge with increased rake angle. As was mentioned previously, the built-up-edge forms more

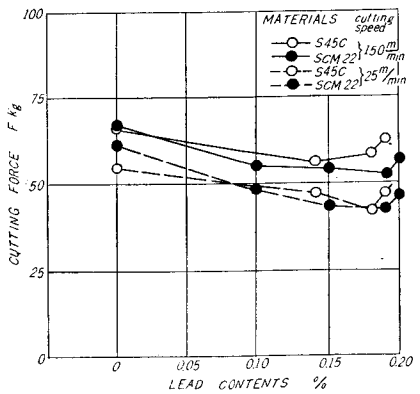

Fig. 13. Variation of cutting force with lead contents.

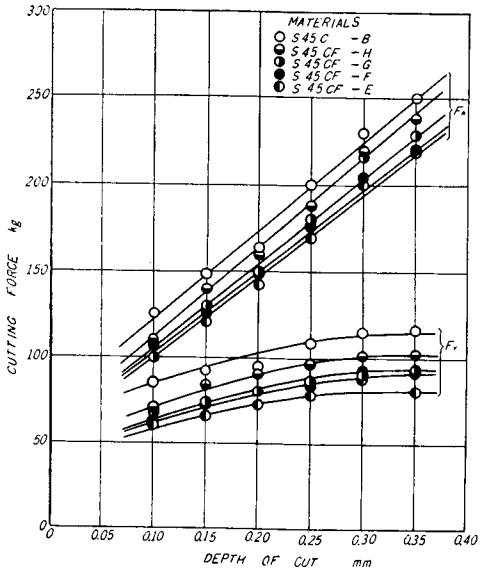

Fig. 14 (a). Effect of depth of cut on cutting force, leaded steels in 45C
Cutting conditions; cutting speed 10 m/min; tool, SKH4; tool geometry, 0, 0, 5, 5, 5, 0, 0:

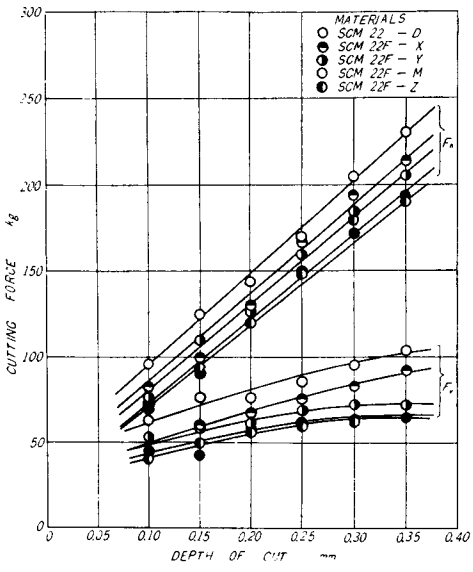

Fig. 14 (b). Effect of depth of cut on cutting force, leaded steels in SCM22
All other conditions were the same as in Fig. 14 (a).

easily with leaded steels than with non-leaded steels. Therefore, the cutting force was greatly affected with leaded steel.

It is found from Figs. 12 (a) (b) that the principal cutting force is smaller and shows a larger variation for leaded steels than for non-leaded steels.

The effect of lead content on cutting force is shown in Fig. 13, the cutting force decreasing with an increase in lead content.

5. 3. Orthogonal cutting tests

5. 3. 1. Cutting force

Principal and feed cutting forces are shown in Fig. 14 (a) (b) in relation to lead content.

5. 3. 2. Coefficient of frictinn on tool face

The coefficient of friction on the tool face was calculated from the two components of cutting force measured in the above experiment, and is shown in Fig. 15 in relation to lead content.

The coefficient of friction was found to decrease with an increase in lead content and depth of cut.

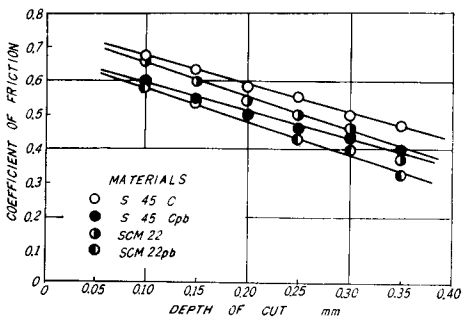

Fig. 15. Effect of depth of cut on coefficient of friction.

6. Machinability based on chip formation

Machinability of leaded and non-leaded steels will be discussed in the following from the standpoint of chip formation, applying the orthogonal cutting principle based upon the flow region concept established by OKUSHIMA and HITOMI.

6.1. Experimental procedure

The sudden-stop orthogonal cutting device shown in Fig. 16 was used to investigate chip formation when cutting free-cutting leaded steels. The cutting was stopped suddenly with this sudden-stop device, after which the specimen was mounted in a mould, polished, and etched in order to observe and photograph the mechanism of chip formation.

Test specimen; leaded steel and non-leaded steel (SCM22) $60 \times 40 \times 2.5$ mm^3

Tool material ; High speed steel (SKH 4)

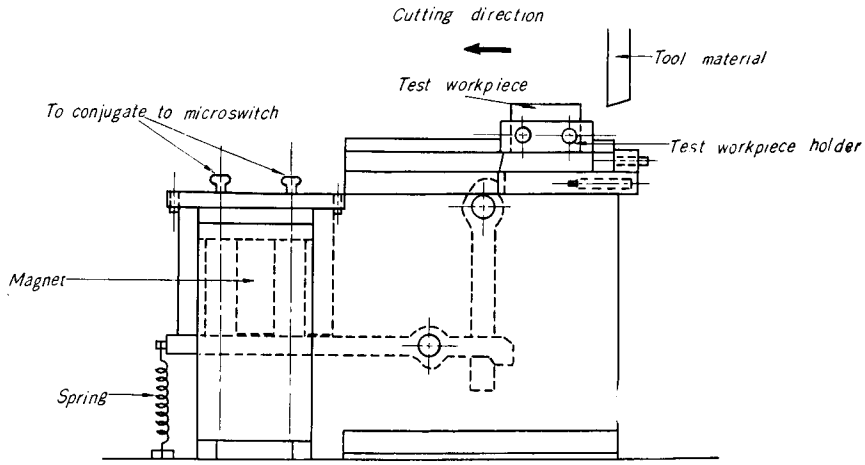

Fig. 16. Apparatus of a sudden-stop orthogonal cutting (main parts).

6.2. Experimental results

The effect of lead content on cutting is shown in Fig. 17. It is evident from this figure that the cutting ratio has a tendency to increase with an increase in lead content and depth of cut. Fig. 18 shows the effect of lead addition on chip contact length on tool face. Chip contact length decreased with an increase in lead content.

6.3. Analysis of the cutting mechanism of free-cutting leaded steels

The cutting mechanism of free-cutting leaded steels was analysed based upon the flow region concept. According to this cutting process chips are produced due to plastic flow in a transitional deformation zone which exists between the work and the chip. (Refer to Fig. 19)

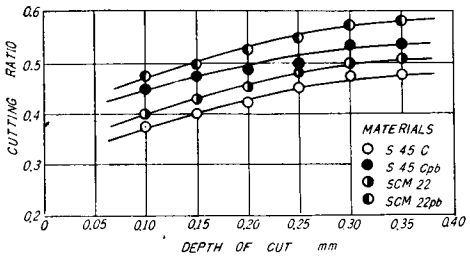

Fig. 17. Effect of depth of cut on cutting ratio.

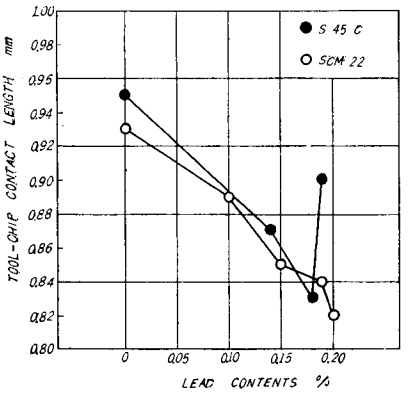

Fig. 18. Variation of tool-chip contact length with lead contents in steels.

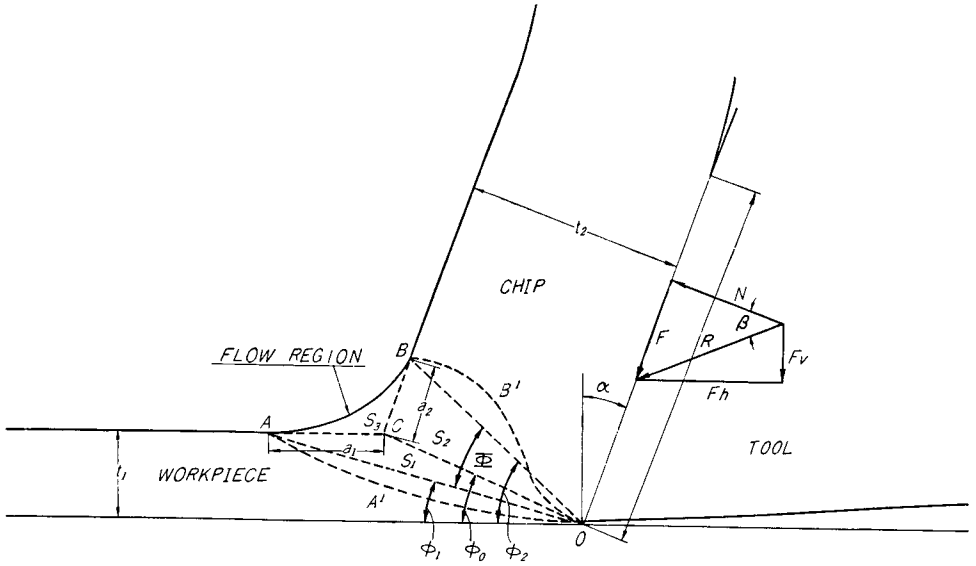

Fig. 19. Analysis of cutting mechanism based on flow rgion concept.

The inclination angles for starting and ending boundary lines and the sector angle of the flow region were deduced theoretically as follows:

$$\phi_3 = \frac{K_1}{2} - \frac{\beta}{2} - \frac{\alpha}{2} \qquad \cdots\cdots(3)$$

$$\phi_1 = \frac{K_2}{2} - \frac{\beta}{2} + \alpha \qquad \cdots\cdots(4)$$

$$K_1 = \sin^{-1}\left\{\frac{2}{k_1}\sin\beta + \sin(\beta-\alpha)\right\} \qquad \cdots\cdots(5)$$

$$K_2 = \cos^{-1}\left\{\frac{2}{k_2}\sin\beta - \sin\beta\right\} \qquad \cdots\cdots(6)$$

$$k_1 = \frac{l}{t_1} \qquad \cdots\cdots(7)$$

$$k_2 = \frac{l}{t_2} \qquad \cdots\cdots(8)$$

$$\varPhi = \phi_2 - \phi_1 = \frac{\alpha}{2} - \frac{K_1}{2} + \frac{K_2}{2} \qquad \cdots\cdots(9)$$

where ϕ_1 is the inclination angle of the starting boundary line of flow region, Deg.
ϕ_2 is the inclination angle of the end boundary line of flow region, Deg.
α is the ranke angle, Deg.
β is the mean friction angle, Deg.
l is the chip contact length, mm.
t_1 is the depth of cut, mm.
t_2 is the thickness of chip, mm.

6. 3. 1. The effect of depth of cut (Figs. 20 (a) (b))

It was found that the inclination angle of the end boundary line of the flow region ϕ_2 and the sector angle of flow region $\varPhi$ increased in direct proportion to the depth of cut. The ratio between chip contact length and depth of cut k_1 and mean friction angle β decreased with an increase in depth of cut. The ratio between chip contact length and chip thickness k_2 and the inclination angle of the starting boundary line of the flow region were constant when depth of cut was changed. It is evident from this that the inclination angle of the starting boundary line ϕ_1 is smaller and that of the end boundary line ϕ_2 is larger than the conventional shear angle. The conventional shear angle ϕ_0 was calculated from the following equation and is shown in Fig. 21.

$$\tan\phi_0 = \frac{r\cos\alpha}{1 - r\sin\alpha} \qquad \cdots\cdots(10)$$

where r is the cutting ratio
α is the rake angle

6. 3. 2. The effect of lead addition (Fig. 21)

With an increase in lead content, angles ϕ_1, ϕ_2 increased, β, k decreased, and k_2, ϕ_1 were almost constant. The sector angle of the flow region area $\varPhi$ showed a tendency to increase with an increase in lead addition. It was found by this result that a smoother shear deformation in the cutting process occurs for leaded steels than for non-leaded steels.

Schematic cutting models for typical SCM 22 steels are shown in Fig. 22 (a) (b).

6. 4. The area of flow region

The variation of cutting mechanism due to lead addition was investigated based upon the size of the flow region for leaded and non-leaded steels in order

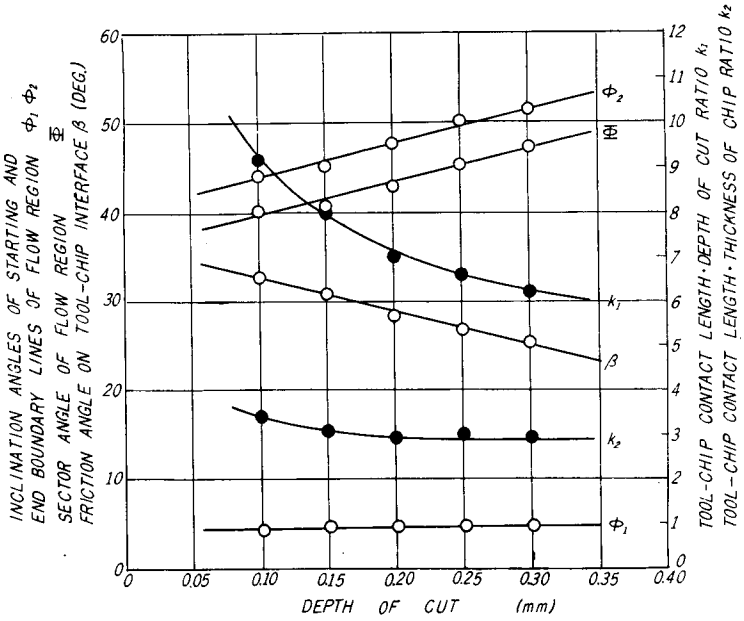

Fig. 20 (a). Calculation value of SCM22 (non-leaded steel) with depth of cut
(Cutting speed, 10 m/min; rake angle, 0 deg; dry).

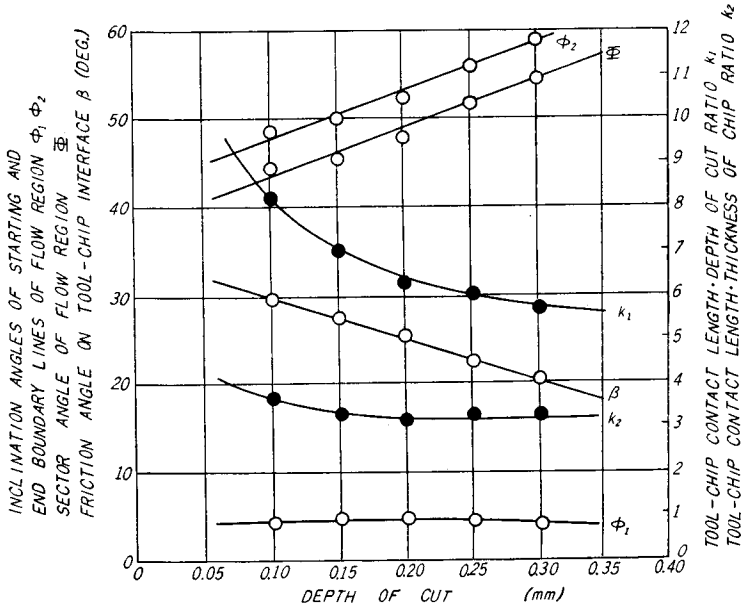

Fig. 20 (b). Calculation value of SCM22 (leaded steel) with depth of cut
(Cutting speed, 10 m/min; rake angle, 0 deg; dry).

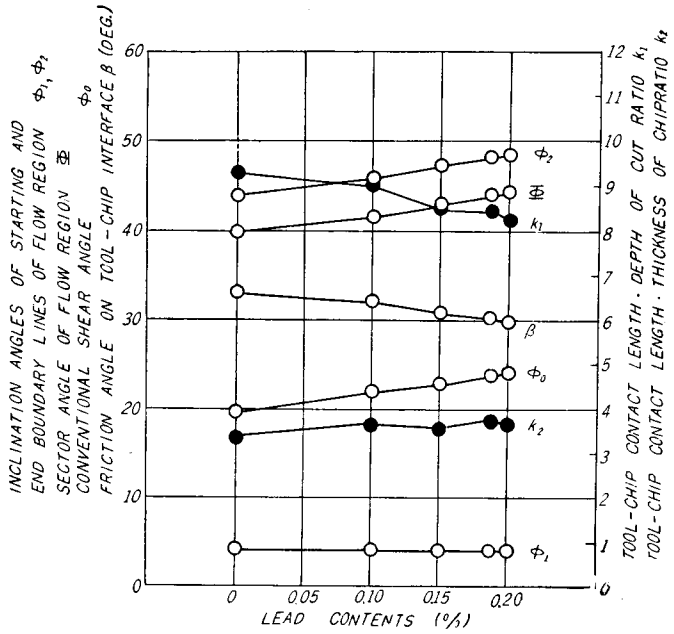

Fig. 21. Calculation value of SCM22 with lead contents.

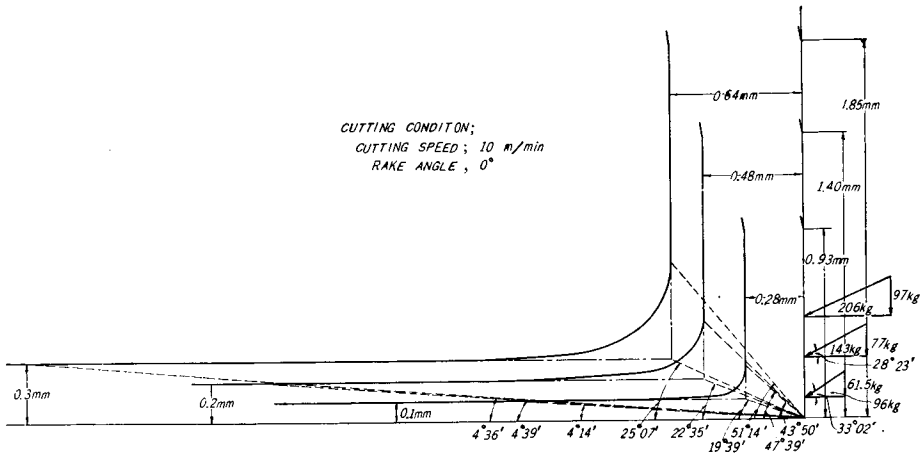

Fig. 22(a). Schematic cutting model for non-leaded steel in terms of depth of cut.

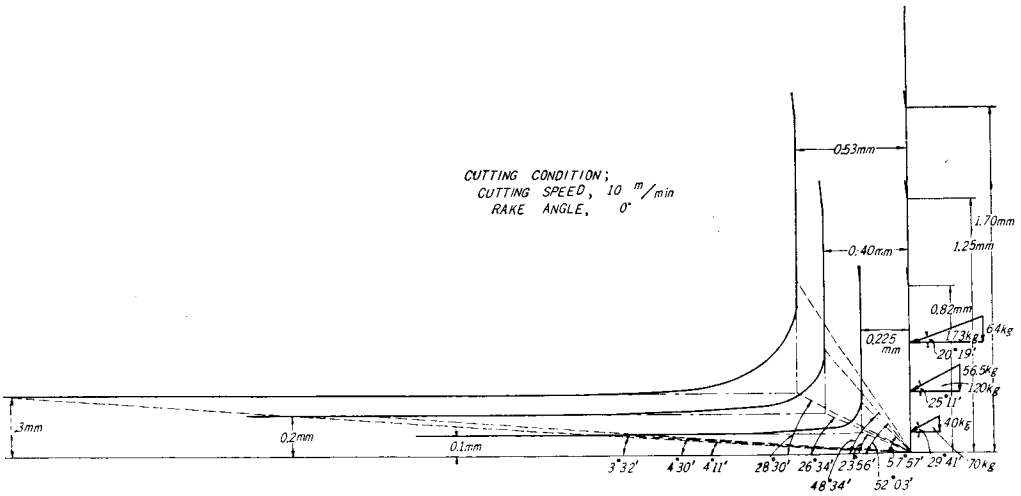

Fig. 22(b). Schematic cutting model for leaded steel in terms of depth of cut.

to determine the effect of including lead in steels. The area AOB of the flow region in the schematic cutting model (Fig. 19) is calculated from the following equation, dividing this area into 3 parts s_1, s_2, and s_3.

$$S = s_1 + s_2 + s_3 \quad \cdots\cdots(11)$$

$$s_1 = \frac{t_1^2}{2}(\cot\phi_1 - \cot\phi_0) \quad \cdots\cdots(12)$$

$$s_2 = \frac{t_1 \cdot t_2}{2} \cdot \frac{\sin(\phi_2 - \phi_0)}{\sin\phi_0 \cos(\phi_2 - \alpha)} \quad \cdots\cdots(13)$$

$$s_3 = \frac{t_2^2}{2}(\tan\varepsilon_0 - \tan\varepsilon) \quad \cdots\cdots(14)$$

$$\tan\varepsilon = \tan(\phi_2 - \alpha) + r^2\cot\phi_1 - (r+1)f - 2f^2\cot\left(\frac{\pi}{4} - \frac{\alpha}{2}\right)\left\{1 - \left(\frac{\pi}{4} - \frac{\alpha}{2}\right)\cot\left(\frac{\pi}{4} - \frac{\alpha}{2}\right)\right\} \quad \cdots\cdots(15)$$

$$f = \frac{a_2}{t_2} \quad \cdots\cdots(16)$$

$$\tan\varepsilon_0 = \tan(\phi_0 - \alpha) + r^2\cot\phi_0 \quad \cdots\cdots(17)$$

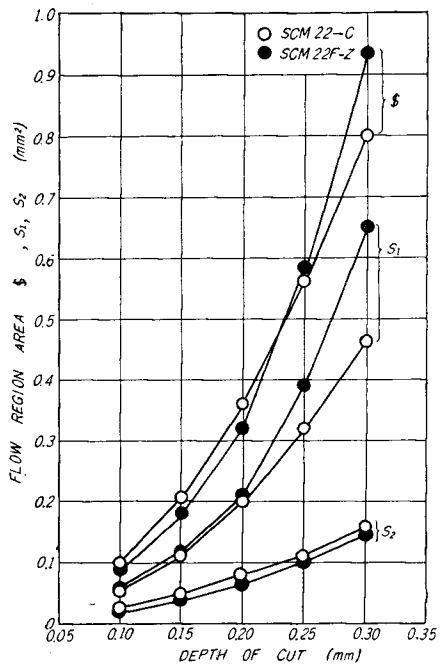

Fig. 23(a). Effect of depth of cut on flow region area.

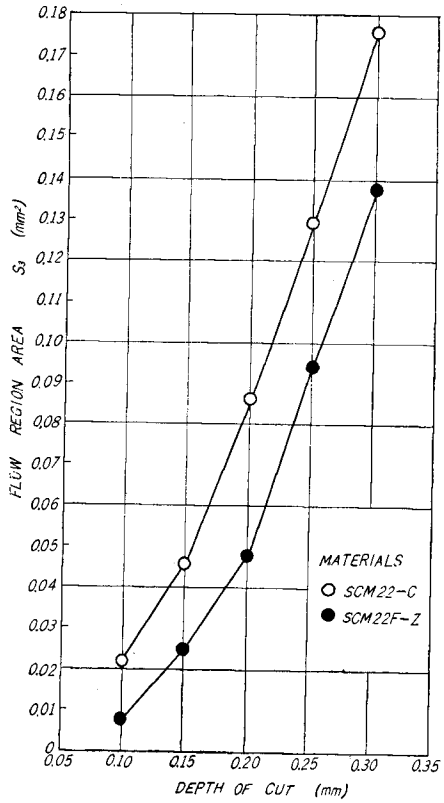

Fig. 23(b). Effect of depth of cut on flow region area.

where r is the cutting ratio

f is the ratio of the size of flow region to chip thickness $=\frac{a_2}{t_2}$

ε = angle between the perpendicular line to tool face and the grid line in steady chip which was formerly perpendicular to the uncut surface

ε_0 = angle of orientation of structure when the chip is formed through a single shear plane

6.5. The area of the flow region for CSM22 steels

The area of the flow region was calculated from the above equations (11)~(17) and is shown in Figs. 23(a)(b). The effect of depth of cut upon the area of the flow region is as follows: when depth of cut is small (e.g. 0.2 mm in this case), the area of the flow region for free-cutting leaded steels, and vice versa will large depth of cut. However, the area s_3 is always larger for free-cutting leaded steels than for non-leaded steels.

Fig. 24 shows the effect of lead content upon the area of the flow region. This areas S decreases with an increase in lead content. It appears that the shear deformation area in metal cutting decreases with lead addition.

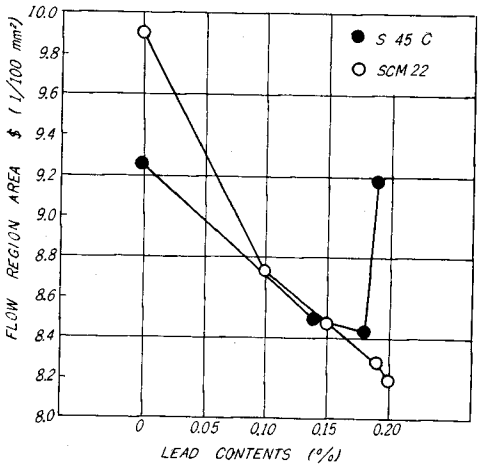

Fig. 24. Effect of lead contents on flow region area.
Depth of cut, 0.1 mm
cutting speed, 10 m/min

7. Conclusions

The above experiments and discussion lead to the following conclusions.

1. Lead inclusion in steels improves machinability from the standpoint of tool life, surface finish, and cutting force.

2. In this experiment and the lead content of the steels varied over a range of 0–0.20%, and the maximum tool life was obtained for a suitable content of lead in a range of 0.10–0.20%.

3. The most suitable tool material when cutting leaded steels was found to be titanium carbide grade A, but grade ST-1 of steel cutting grade carbide was also effective.

4. Lead inclusion in steels improved the surface finish, but this effect was not recognized at low speeds below 100 m/min., and at low feeds.

5. The difference in cutting between free-cutting leaded steels and non-leaded steels was very promment at the lower speeds below the minimum cutting speed for a constant surface roughness.

6. Lead in SCM22 and S45C improved machinability from the standpoint of chip formation, that is, principal and feed cutting forces, chip contact length on tool face and chip thickness decreased and shear angle increased with an increase in lead content.

7. The cutting mechanism of free-cutting leaded steels was analysed based upon the flow region concept.

The effects of depth of cut and lead content on the cutting process were discussed.

It was found that a smoother shear deformation occurs in the cutting process for leaded steels than for non-leaded steels, and that hence the inclusion of lead in steels improves machinability.